



Cite this: *J. Mater. Chem. B*, 2020,
8, 1897

Self-assembling RATEA16 peptide nanofiber designed for rapid hemostasis

Shuda Wei,^a Fangping Chen, *^{ab} Zhen Geng, ^a Ruihua Cui,^a Yujiao Zhao^a and Changsheng Liu *^{ab}

Uncontrolled bleeding remains a contributor of mortality in various accidents, and ideal hemostatic materials with rapid and efficient hemostasis, ease of use, biocompatibility and non-toxic characteristics are urgently needed. In this study, we synthesized a novel polypeptide material, RATEA16 ($\text{CH}_3\text{CO-RATARAEARATARAECO-NH}_2$), by the solid phase method, and investigated the secondary structure, self-assembly performance, gelation ability, biocompatibility and hemostatic efficiency *in vitro* and *in vivo*. The results showed that the RATEA16 peptide solution had an appropriate pH after replacing the strongly acidic aspartic acid with weakly acidic Glu and basic Thr in the RADA16-I backbone. The secondary structure of RATEA16 played an important role in the formation of nanofibers induced by self-assembling behavior. RATEA16 possessed good biocompatibility and rapid gelation ability. Animal liver model experiments showed that RATEA16 had a higher blood coagulation rate than CMS and Arista[®] and achieved complete hemostasis in about 40 seconds. Therefore, the study indicated that the self-assembled peptide RATEA16 had excellent biocompatibility and efficient hemostasis, suggesting that RATEA16 can serve as a reliable and promising hemostatic agent for rapid hemostasis.

Received 17th November 2019,
Accepted 20th January 2020

DOI: 10.1039/c9tb02590a

rsc.li/materials-b

Introduction

Uncontrolled hemorrhaging is one of the major causes of death induced by surgery, battle and disaster emergencies.¹ The body's natural response to injury includes the formation of platelet embolisms, the formation of fibrin resulting from the enzymatic cascade, the dissolution of blood clots and the healing of wound sites.^{2,3} However, massive hemorrhages cannot be stanched by only relying on the natural response of blood itself. Therefore, it is important to develop rapid and effective hemostatic materials to improve the survival rate and the quality of life of the wounded.

Many efforts have been exerted to develop various hemostatic agents. Some are clinically applied, such as dry fibrin sealant dressings (Porcine Fibrin Sealant Kit[®]), chitosan dressings (HemCon[®]) and zeolite dressings (QuikClot[®]),^{4–6} but there are still inevitable defects. Fibrin hemostatics have a short shelf life and insufficient environmental adaptability, which limits their applications.^{7,8} Chitosan has poor stability and limited hemostasis ability.^{9–11} Zeolites exhibit undesirable exothermic damage and inferior biodegradability.^{12–14} Consequently, it is imperative to explore ideal hemostatic materials combined with rapid and

efficient hemostasis, ease of use, biocompatibility and non-toxic characteristics.^{7,15–17}

Peptide hydrogel hemostatics have received much attention due to their inherent biocompatibility and self-assembly characteristics.^{18–21} Previous studies showed that self-assembled peptides achieved complete hemostasis in a short time by forming nanofiber barriers and concentrating the tangible blood components when applied directly to wounds.¹⁸ RADA16-I is a typical self-assembled peptide, with a primary peptide sequence of $\text{CH}_3\text{CO-RADARADARADARADA-CO-NH}_2$.^{22–24} With a high propensity to form highly stable β -sheet structures, RADA16-I can spontaneously self-assemble into high-order nanofibers with high water content.²¹ The formed nanofiber entanglements entrap blood components such as red blood cells and platelets.¹⁹ Meanwhile, the peptide transforms into gels and can be applied on wounds, which makes the patient stop bleeding rapidly. Furthermore, the peptide can be degraded into carbamide eventually and excreted by the human circulatory system. However, the self-assembled peptide RADA16-I solution has the deadly drawback of a low pH value of about 3–4, which could damage cells and lead to cytotoxicity or even sterile inflammation upon direct injection.^{25–28}

Amino acid types and peptide sequences play a pivotal role in the hydrophobic and hydrophilic properties, acid-base properties and molecular weight of peptide chains.²⁹ Takatoshi³⁰ found that a new peptide was pH-responsive on replacing the acidic amino acids in the RADA16-I sequence, and the modified peptide was named RATEA16. When the solution changed from

^a Engineering Research Center for Biomedical Materials of Ministry of Education, East China University of Science and Technology, Shanghai 200237, P. R. China.
E-mail: fpchen@ecust.edu.cn

^b The State Key Laboratory of Bioreactor Engineering, East China University of Science and Technology, Shanghai 200237, P. R. China

acidic to alkaline, the peptide liquid underwent a change from solution to gel and eventually to precipitate. However, RATEA16 has not been used in tissue repair and hemostasis. The peptide RADA16-I contains a considerable number of aspartic acid (strongly acidic amino acid) residues which leads to the low pH value. Whether the acid problem could be alleviated and the modified peptide could still retain its self-assembly properties on substituting the aspartic acid with threonine (neutral amino acid) and glutamic acid (weakly acidic amino acid) was still unknown.

Herein, aiming to up-regulate the pH value to neutral and not to affect the self-assembling ability, we developed a half-sequence ionic-complementary self-assembled peptide, RATEA16 ($\text{CH}_3\text{CO}-\text{RATARAEARATARAEA}-\text{CONH}_2$), which was obtained by solid-phase synthesis, by modifying the aspartic acid in RADA16-I to threonine and glutamic acid. RATEA16 is composed of regular repeating residues containing arginine (Arg), alanine (Ala), threonine (Thr) and glutamic acid (Glu). As a result, the pH value increased remarkably, reaching 6–7. This important deficiency was resolved successfully. In addition, RATEA16 was tested and characterized by other methods like HPLC, TOF-MS, CD, AFM and TEM. Then, the hemostatic performance and biocompatibility of the RATEA16 peptide were evaluated.

Experimental procedures

Materials

The peptide RATEA16 ($\text{CH}_3\text{CO}-\text{RATARAEARATARAEA}-\text{CONH}_2$) was synthesized by solid-phase synthesis. The N-terminus and C-terminus were protected by amino and acetyl groups, respectively (molecular weight 1712.9 Da). The crude peptide was purified by high performance liquid chromatography (HPLC). Peptide homogeneity and composition were analyzed by matrix-assisted laser desorption/ionization time of flight mass spectrometry (MALDI-TOF-MS). Peptide stock solutions with 1% (wt/vol; 10 mg mL⁻¹) concentration were prepared in Milli-Q water (18.2 MΩ cm) and stored at 4 °C. The pH value was tested with a precision pH test paper.

CD measurements

CD measurements were conducted at 25 °C using a 1 mm path length quartz cuvette. Spectra were collected at 2 nm intervals and band widths of 2 nm from 190 to 260 nm at 3 s signal intervals. The baseline CD signals of an empty cuvette and a cuvette containing pure water were checked. The concentrations of peptide solutions for the CD measurements were 0.1 mg mL⁻¹ and 0.25 mg mL⁻¹.

FTIR characterization

FTIR was carried out on a Nicolet IS50 instrument. RATEA16 peptide prepared in D₂O was placed on a CaF₂ plate and dried in vacuum. The spectra were collected in absorbance mode from 4000 cm⁻¹ to 1000 cm⁻¹.

AFM and TEM observations

AFM in tapping mode was used to observe the nanostructure of the peptide using an RTESP (Veeco) instrument. 5 μL peptide

solution was deposited on a fresh cleaved mica surface and kept for 20 s. After washing with 200 μL of Milli-Q water, the samples were air-dried.

TEM was used to observe the microscopic morphology of the self-assembled peptide nanofibers using a JEM-2100 (JEOL) instrument. Before the observation, a solution of peptide was loaded onto a copper grid with a carbon supported film and stained with sodium phosphotungstate.

Gelation ability on contact with blood

20 μL transparent RATEA16 peptide solution (5 mg mL⁻¹) was dropped onto 50 μL fresh blood in a dry and clean glass dish to investigate its gelation ability when it contacted blood. Fresh blood was collected from the ear veins of healthy New Zealand rabbits and stored in an anticoagulant tube with 3.8% sodium citrate.

Red blood cell adhesion

The adhesion ability and morphology of red blood cells incubated with the peptide were monitored by environmental scanning electron microscopy (ESEM, Quattro C, Thermo Scientific, USA). The stock RATEA16 solution was diluted to 5 mg mL⁻¹ with deionized water. Subsequently, 50 μL RBCs along with 100 μL RATEA16 solution were incubated at 4 °C for 30 min. The anticoagulated fresh blood was centrifuged at 3000 rpm for 15 min at 4 °C and the red blood cells were reacquired by discarding the supernatant. PBS buffer (pH 7.4) was added to remove the unstuck red blood cells.

TEG assay

The coagulation efficiency in whole blood and the induced thrombotic effects were evaluated by thromboelastography (TEG-5000[®], Haemoscope Corporation, Niles, IL) supported by East Hospital affiliated to Shanghai Tongji University. Citrated whole blood collected from a healthy donor was provided by the hematology department of Shanghai Oriental Hospital. 100 μL 5 mg mL⁻¹ RATEA16 was incubated with 340 μL citrated whole blood in a cuvette, and then 20 μL 0.2 mol mL⁻¹ CaCl₂ solution was introduced. A negative control without samples was included and the test was carried out at 37 °C. TEG parameters include: (1) reaction time *R*; (2) coagulation time *K*; (3) rate of clot polymerization or rapidity of fibrin cross-linking, *α*-angle; and (4) maximum amplitude or maximum clot strength MA.^{31,32}

Biocompatibility evaluation

An erythrocyte PBS suspension with 10% hematocrit was prepared in advance. The peptide powder was completely dissolved in PBS by ultrasonication to form RATEA16 at different concentrations (0.5 mg mL⁻¹, 1 mg mL⁻¹, 2 mg mL⁻¹, and 5 mg mL⁻¹). 100 μL PBS and 100 μL deionized water were selected as a negative control group and a positive control group, respectively (*n* = 3). 100 μL of the red blood cell suspension was added. After incubation at 37 °C for 1 h, each group was centrifuged at 3000 rpm for 15 min at 4 °C. 150 μL supernatant was added to a 96-well plate. The amount of hemoglobin released and the

degree of damage to the red blood cells were characterized by a microplate reader at 540 nm absorbance. The hemolysis ratio was calculated according to eqn (1).

$$\text{Hemolysis ratio (\%)} = (A_n - A_t)/(A_p - A_t) \times 100\% \quad (1)$$

where A_n , A_t and A_p represent the OD values at 540 nm of the samples, the negative control group and the positive control group, respectively.

The MTT assay was used to evaluate the cytotoxicity of RATEA16. L929 fibroblasts were used as the experimental cells. DMEM without fetal bovine serum was used to prepare the RATEA16 peptide solution (2 mg mL^{-1}). The extract was sterilized through a $0.22 \mu\text{m}$ sterile filter. After the L929 fibroblasts were cultured in DMEM in a fully humidified atmosphere of $5\% \text{ CO}_2$ at 37°C for 12 hours, $100 \mu\text{L}$ sterile extract was added and incubated for 24 hours, 48 hours and 72 hours. The cell viabilities were evaluated by the MTT assay.

Three parallel experiments were carried out for each group and the results were averaged.

Hemostatic ability *in vivo* and histologic evaluation

The rabbit (white male New Zealand rabbits, 2–4 kg, Jiagan Biotechnology Co. Ltd, Shanghai, China) liver hemorrhaging model was selected to evaluate the *in vivo* hemostatic ability of the RATEA16 peptide. All animal experimental protocols and animal care were approved by the animal investigation ethics committee of Jiagan Biotechnology Co. Ltd. The rabbits were supplied only with water for 12 h before the operation, and received general anesthesia with pentobarbital sodium (30 mg kg^{-1}) by intravenous injection. The samples (10 mg mL^{-1}) were sterilized by a filter membrane ($0.22 \mu\text{m}$). In this study, oxidized microporous starch (OMS) was employed as a negative control group and sterilized by ultraviolet radiation (Heming Co. Ltd, Shanghai, China). Arista® styptic powder (Medafor, USA) was set as the positive control group.

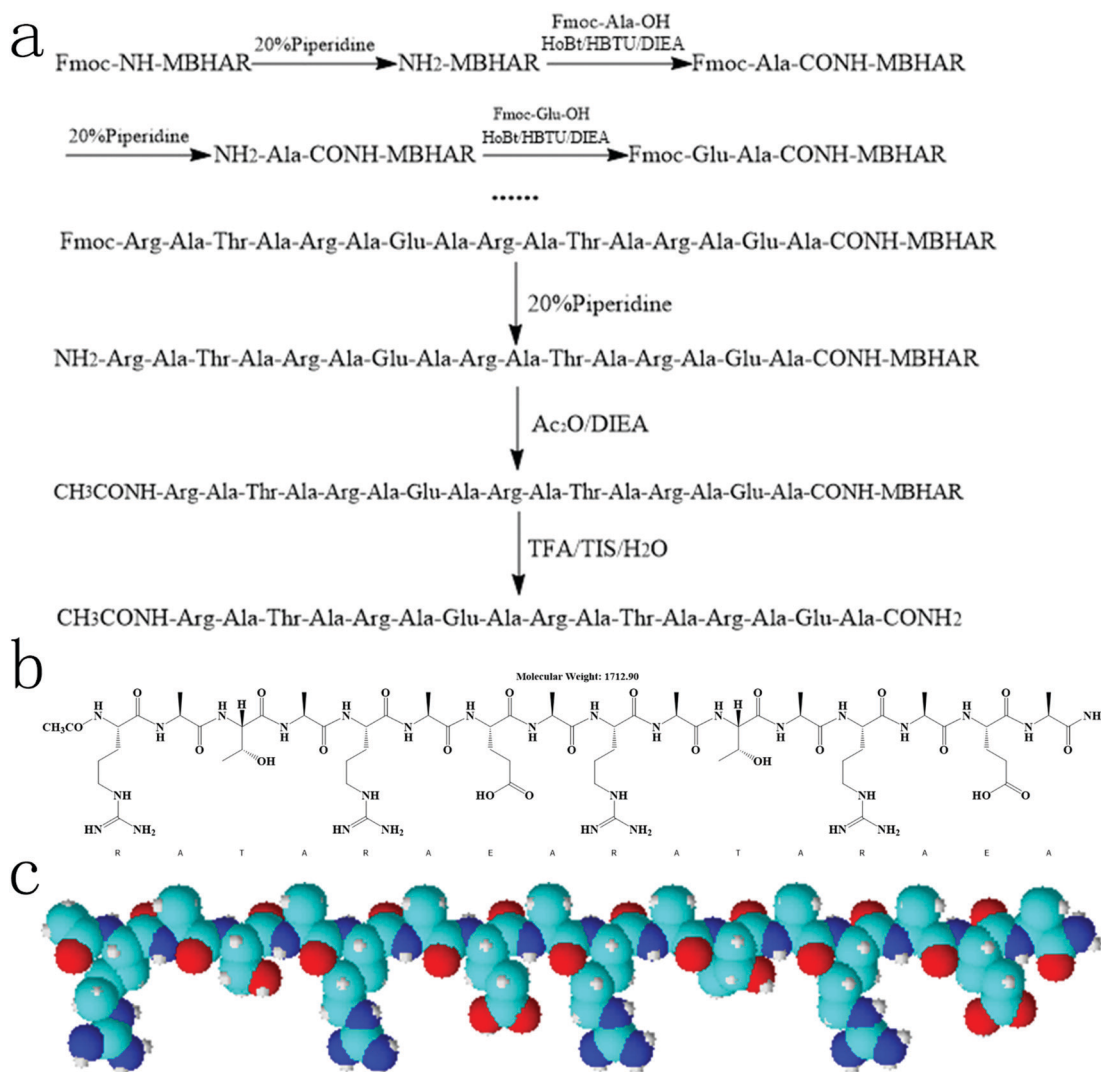


Fig. 1 (a) Schematic representation, (b) molecular formula and (c) three-dimensional sphere structural formula of RATEA16 obtained by solid-phase synthesis (blue, red, turquoise and white represent nitrogen atoms, oxygen atoms, carbon atoms, and hydrogen atoms, respectively).

The hair of the rabbits was initially shaved off to expose the abdomen after anesthesia. The left lobe of the liver was cut transversely ($1\text{ cm} \times 2\text{ mm}$) using a No. 15 scalpel, and the transudatory blood from the wound surface was absorbed by pre-weighted gauze. Immediately, $100\text{ }\mu\text{L}$ RATEA16 (10 mg mL^{-1}) was injected into the bleeding site. OMS and Arista[®] were sprayed directly onto the wound as controls. The bleeding time was recorded and the bleeding mass was calculated. All experiments were performed in triplicate.

The postoperative rabbits were monitored for 7 days to observe the survival rate. The rabbits were anesthetized on day 7 and the lobe of the liver where hemostasis had been applied was exposed. The wounds were examined and photographs were taken. Subsequently, the rabbits were euthanized and specimens from the wound sites were harvested. Specimens were fixed in formalin and embedded in paraffin for H&E staining.³³

Results and discussion

Characterization of RATEA16 peptide

Fig. 1a shows a schematic representation of the preparation of the RATEA16 peptide by solid-phase synthesis. RATEA16 was composed of arginine (Arg), alanine (Ala), threonine (Thr) and glutamic acid (Glu) in a regular sequence. Fig. 1b and c depict the molecular formula and the corresponding three-dimensional sphere structural formula, respectively. The molecular weight and purity of the RATEA16 peptide were detected by TOF-MS and HPLC. Fig. 2a shows an experimentally measured molecular weight of 1712.9, which was consistent with the theoretical molecular weight of 1712.9, indicating that the peptide was synthesized successfully. Fig. 2b only shows one peak in the HPLC graph at 7.557 min, demonstrating that the purity of RATEA16 met the requirements.

Increasing the pH value is the main aim of this study. RATEA16 was fabricated by replacing the strongly acidic aspartic acid with weakly acidic Glu and basic Thr in the RADA16-I backbone. Interestingly, at the same concentration of 1 mg mL^{-1} , the pH of a RATEA16 peptide solution reached 6, twice as high as that of a RADA16-I peptide solution (pH 3–4).

Secondary structure

Circular dichroism (CD) is used to evaluate the secondary structure, folding and binding properties of proteins, as different structural elements have unique CD spectra at a particular wavelength. For instance, α -helical proteins have negative Cotton bands at 205–210 nm and 215–225 nm and a positive Cotton band at 190–195 nm. On the other hand, proteins with well-defined antiparallel β -pleated sheets (β -helices) have negative Cotton bands at 210–220 nm and positive Cotton bands at 192–200 nm, while disordered protein structures display low ellipticity at 215–220 nm and negative bands near 195–200 nm.³⁴ Fig. 3 reveals the secondary structure of RATEA16 by CD spectroscopy and exhibits a strong positive band at 195 nm and a negative band at 215 nm, which are typical features of the β -sheet structure.³⁵ Thus, the CD spectra demonstrated on the molecular scale the key structural component of our designed self-assembling peptide used to drive assembly into fibers. It was obvious that RATEA16 nanofibers are rich in the β -sheet structure. FTIR spectroscopy was used to further investigate the secondary structure. Fig. 4 displays an obvious absorption peak at 1657 cm^{-1} , which was assigned to intermolecular β -sheets of peptides.^{36,37} The result coincided with the CD results for RATEA16.

Micromorphology characterization of RATEA16 nanofibers

AFM was used to observe the microstructure of the designed self-assembled peptides.³⁸ Fig. 5 shows the emergence of nanofibers, and indicates that the RATEA16 peptide formed a long and dense self-assembled nanofiber. As the peptide solution concentration became larger, the diameter of the nanofibers formed by self-assembly became thicker. The results confirmed the excellent self-assembly ability of the RATEA16 peptide.

TEM was used to observe the morphologies of the self-assembled peptides, using sodium phosphotungstate as a negative stain. Ribbon-like nanofibers were observed in the RATEA16 peptide solution (Fig. 6), which was similar to the morphology of RADA16-I reported previously.²⁸

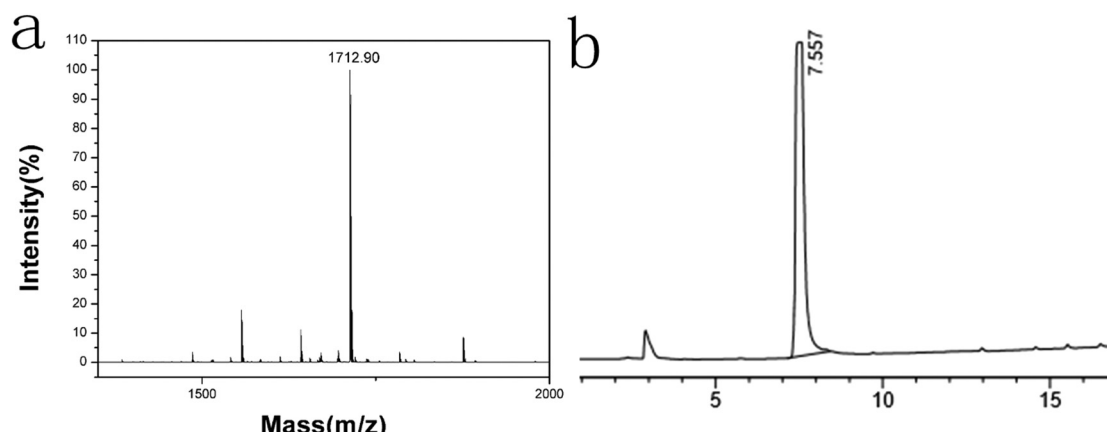


Fig. 2 (a) TOF-MS spectrum and (b) HPLC chromatogram of RATEA16.

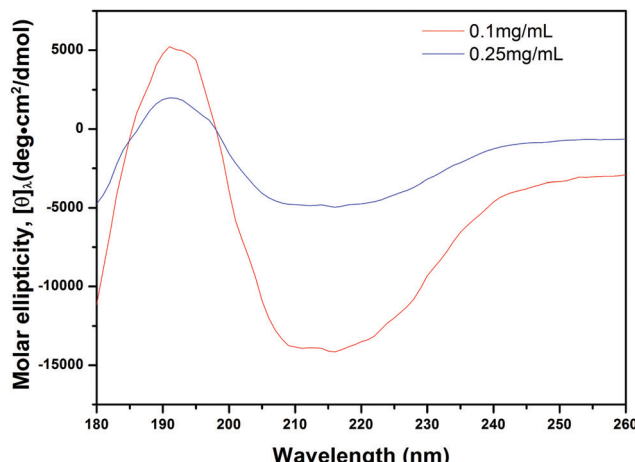


Fig. 3 CD chromatogram of RATEA16 at two concentrations.

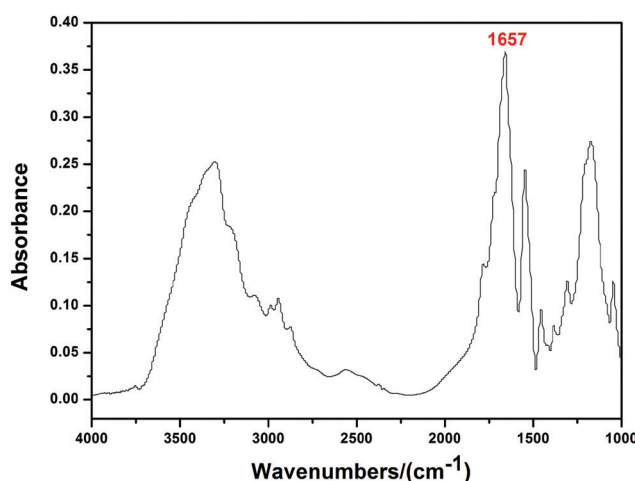


Fig. 4 The Fourier transform infrared spectrum of RATEA16.

Gelation ability

Gelation ability is a critical factor for liquid hemostatic materials in order to stop bleeding. 50 μ L anticoagulated blood was added to 20 μ L 5 mg mL⁻¹ RATEA16 solution, and the blood fluidity was

instantly reduced. After contact for 5 s, RATEA16 spread out along the area where the blood flowed. More importantly, a glue membrane was seen to form and attach to the glass dish, and the red blood cells were wrapped in membranes (Fig. 7a-d).

With the addition of 20 μ L RATEA16 solution to the blood, a gel was rapidly formed. The color of the blood around the gel became darker after contact for 2 s, indicating that the formed nanofibers had an adsorption effect on the aggregation of red blood cells (Fig. 7e-h). In addition, spherical gels were formed and stuck to the bottom of the glass dish (after contact for 4 s). The difference in gel formation ability may relate to the blood flow. Meanwhile, the nanofibers constructed a three-dimensional net structure under blood stimulation.

RBS adhesion

The RATEA16 peptide displayed great gelation ability for rapidly concentrating the tangible blood components. Fig. 8a clearly shows the aggregation and attachment of red blood cells on the RATEA16 surface. Perhaps this is related to the rough surface of the peptide nanofibers. More interestingly, obvious three-dimensional network structures were observed and a large net was created which provided adhering sites for red blood cells. (Fig. 8b). Meanwhile, the formed nanofiber net exhibited a strong capacity to trap the red blood cells as natural fibrin clots and accelerate blood coagulation.

TEG

TEG characterizes *in situ* the viscoelastic properties of blood clots during the coagulation process. We evaluated the formation and strength of a blood clot on the RATEA16 peptide as a function of time. The TEG data are provided in Table 1 and Fig. 9. There was no obvious difference in MA between the control group and RATEA16. The *R* value represented the period of time from coagulation initiation to initial fibrin formation, reflecting the time to form the first fibrin clot. It was observed that the *R* value decreased from 8.5 min to 6.3 min in the presence of RATEA16, indicating that the blood coagulation initiation time of RATEA16 is shorter. In addition, the *K* value decreased sharply and the α value increased significantly in the presence of RATEA16, indicating that RATEA16 possessed a higher coagulation rate and accelerated the

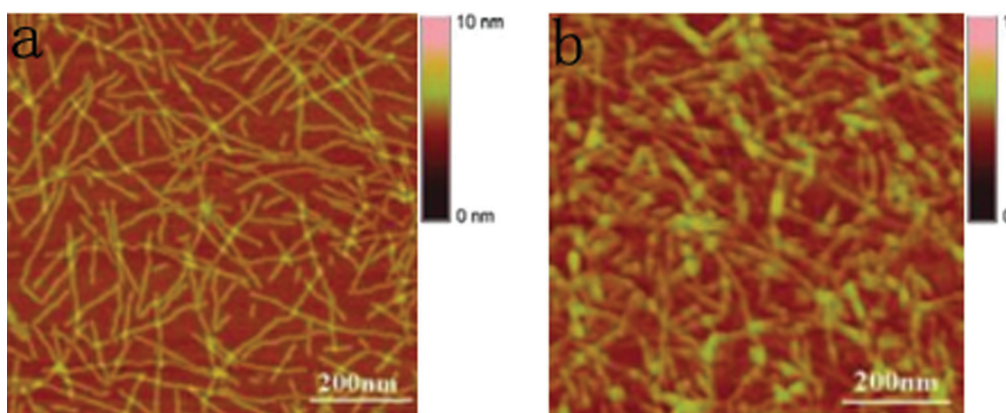


Fig. 5 AFM phase images of the RATEA16 peptide. (a) 1 mg mL⁻¹. (b) 2 mg mL⁻¹.

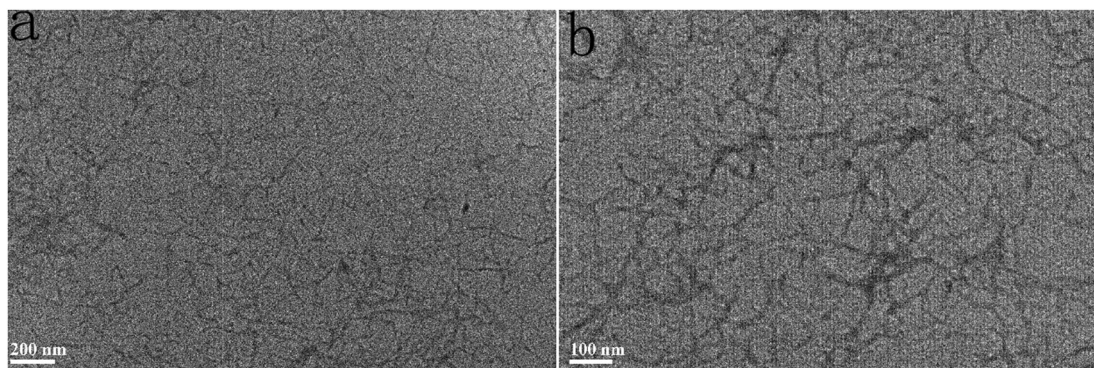


Fig. 6 TEM images of the RATEA16 peptide with negative staining at room temperature. (a) 200 nm, (b) 100 nm.

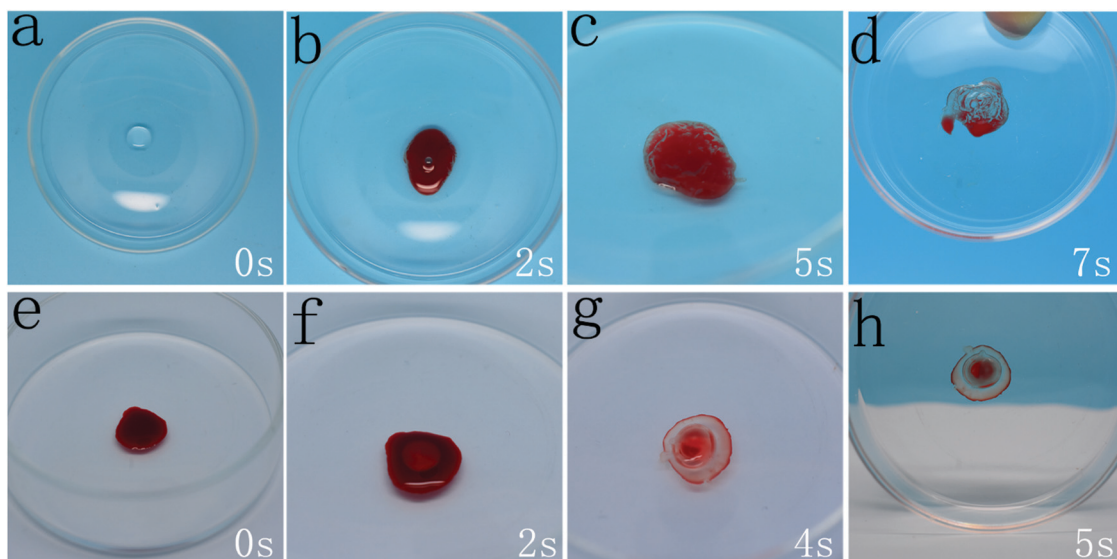


Fig. 7 The gelatinization of RATEA16 in blood: (a–d) the blood was added to the peptide; (e–h) the peptide was added to the blood.

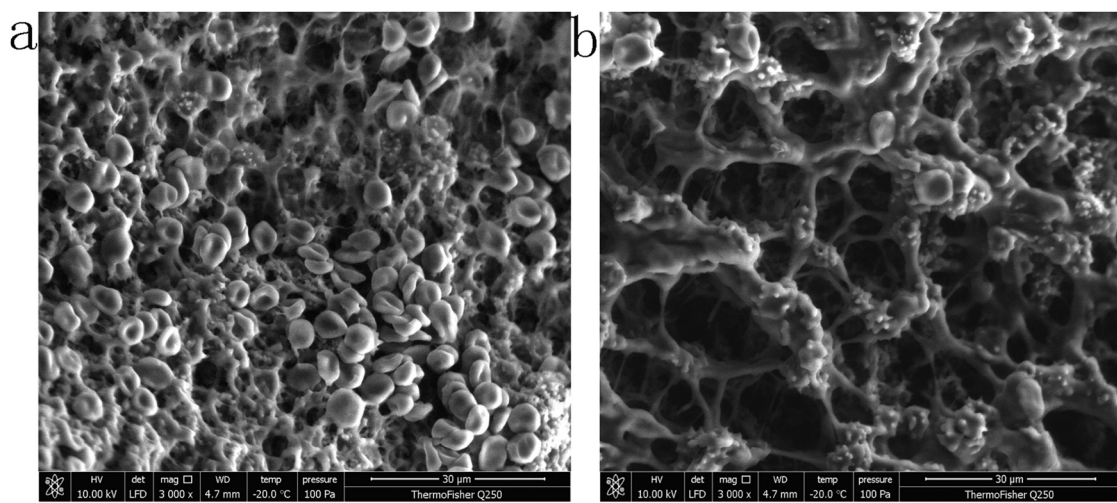


Fig. 8 (a) Aggregation and attachment of red blood cells on RATEA16. (b) Three-dimensional network structure of RATEA16.

subsequent blood coagulation. The influence of RATEA16 on the whole blood clotting process may be due to a phase transformation

of the peptide, which increased the blood viscoelasticity and the concentration of platelets and RBCs.

Table 1 Clotting kinetic parameters of blood mixed with RATEA16 peptide

Material	R (min)	K (min)	α (deg.)	MA (mm)
Control	8.5	5.8	38.7	63.5
RATEA16	6.3	2.5	58.2	62.3

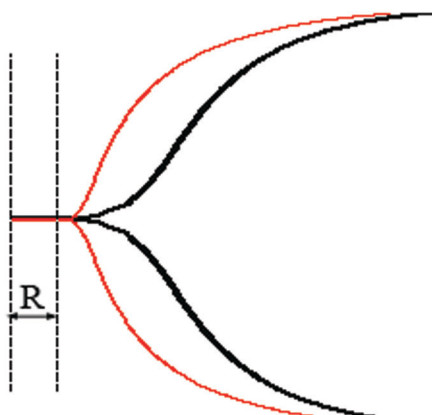


Fig. 9 The TEG image (the black line represents the control; the red line represents RATEA16).

Biocompatibility of RATEA16 peptide

To explore the biocompatibility of the RATEA16 peptide, erythrocyte and L929 fibroblasts were used for the hemolysis analysis and the MTT assay, respectively. As shown in Fig. 10a, a red blood cell PBS suspension incubated on the RATEA16 peptide presented extremely feeble hemolysis. The hemolysis ratios of peptides at concentrations of 0.5 mg mL^{-1} , 1 mg mL^{-1} , 2 mg mL^{-1} , and 5 mg mL^{-1} were $(0.34 \pm 0.025\%)$, $(0.05 \pm 0.0035\%)$, $(0.32 \pm 0.033\%)$ and $(0.07 \pm 0.0046\%)$, respectively, and were much lower than the safety standard of 5%. There was no significant difference in the hemolysis ratio on moving from 0.5 mg mL^{-1} to 5 mg mL^{-1} . The hemolysis ratio remained low even at high concentration of peptide. The result further

indicated that the RATEA16 peptide solution had good hemocompatibility.

We further evaluated the cytocompatibility of the RATEA16 peptide with L929 fibroblasts using a microplate reader. Fig. 10b shows the OD values. Compared with the control, the L929 cells incubated on the peptide exhibited high activity and significant proliferation after 24 h and 48 h, with the cell viabilities reaching 106% and 108%, respectively. This could be explained by the RATEA16 peptide undergoing a preliminary decomposition during the cell growth process, and then degrading into short-chain amino acids, which were used as nutrients for cell growth. This shows that the material had no stimulative effect on the cells. After culturing for 72 h, the cell viability of RATEA16 decreased, but retained an acceptable level of about 85%. Overall, the results showed that RATEA16 had good biocompatibility.

Haemostatic efficiency *in vivo*

The haemostatic efficiency of the RATEA16 peptide *in vivo* was investigated using rabbit liver models. OMS and Arista[®] were selected as the control groups. It is worthwhile to demonstrate that RATEA16 (liquid material) displayed a better performance than OMS and Arista[®] (powder materials). As shown in Fig. 11c, the wounds treated with RATEA16 rapidly achieved control of bleeding in 42.25 ± 1.63 s, whereas the wounds treated with OMS and Arista[®] stopped bleeding after 150 ± 4.16 s and 139 ± 3.95 s, respectively. In addition, the blood loss for RATEA16 was 1.6 ± 0.3 mL, whereas those for OMS and Arista[®] were 2.5 ± 0.5 mL and 2.4 ± 0.4 mL, respectively.

The bleeding of the liver was monitored by taking photographs of the haemorrhaging site at different operation periods (Fig. 11a and b). When the peptide was injected into the bleeding site, RATEA16 immediately turned into a gel and quickly adhered to the wound. After the floating blood was absorbed, the wound was covered by transparent gel membranes. A large number of red blood cells gathered in the wound centre and formed blood clots, which was not found in the control group. Inevitably, the powder type haemostatic materials would cover the liver, which is not conducive

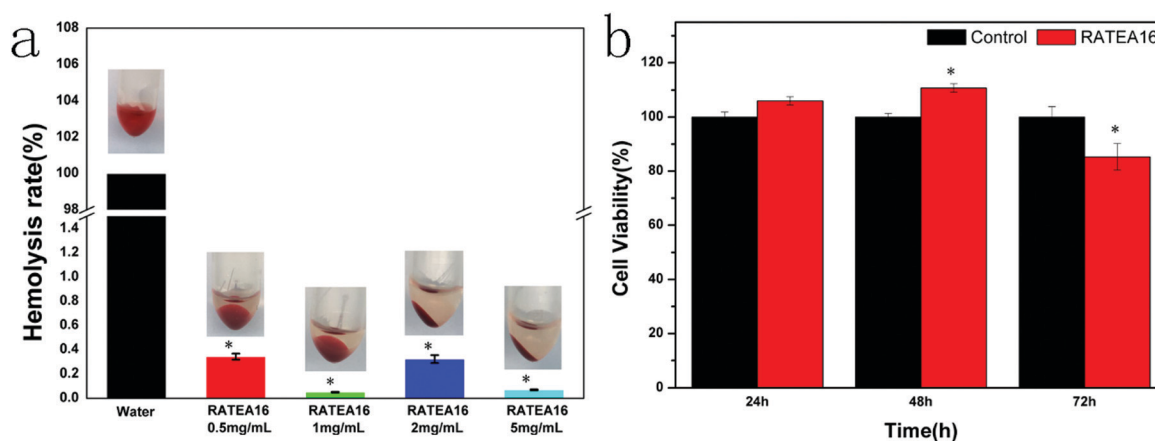


Fig. 10 The biocompatibility of RATEA16 peptide. (a) The hemolysis ratio of materials at different concentrations. (b) The proliferation of L929 fibroblasts cultured in the extraction materials. The symbol (*) denotes statistical significance compared to the relevant control ($P < 0.05$). Data are represented as the mean \pm SD ($n = 3$).

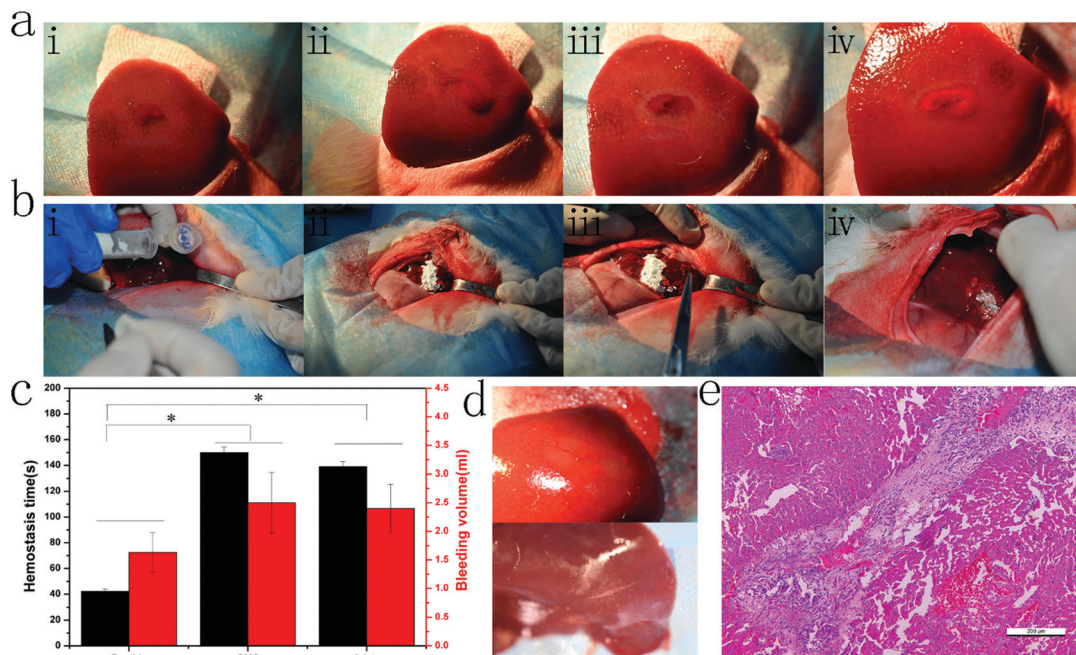


Fig. 11 *In vivo* hemostatic evaluation. The hemostatic period using (a) RATEA16 and (b) Arista®. (i) Blood gushing from the “—” shaped trauma surface. (ii) Applying the hemostatic materials on the wound. (iii) The hemostatic process. (iv) Complete hemostasis. (c) Hemostasis time and bleeding volume of different materials in the liver hemostasis model. (d) Wound recovery of the liver hemostasis model. (The photo at the top shows the wound after hemostasis, and the bottom photo shows the wound seven days after surgery). (e) Hepatic hemorrhage and surrounding tissue by H&E staining after 1 week. The symbol (*) denotes statistical significance compared to the relevant control ($P < 0.05$). Data are represented as the mean \pm SD ($n = 3$).

to intraoperative observation and postoperative removal. On the contrary, RATEA16 formed a transparent gel and was easily degraded, avoiding causing secondary damage to the wound and allowing the haemostasis to be observed in real time.

As mentioned above, RATEA16 exhibited more efficient and rapid haemostasis than OMS and Arista®. The haemostatic mechanism of RATEA16 is not very clear currently. It could be explained by the RATEA16 nanofibers transforming into a three-dimensional net structure to trap the blood components, accelerating the formation of blood clots. Meanwhile, the RATEA16 peptide could form a gel film, adhere tightly to the wound and plug the bleeding site.

7 days after surgery, the wounds had mainly recovered well. The H&E section examination shown in Fig. 11e further supported the excellent wound healing. The result indicated that the RATEA16 peptide not only stopped the bleeding rapidly but also exhibited a remarkable wound repair property.

Conclusions

This study reported a novel self-assembling RATEA16 peptide nanofiber based on RADA16. The pH value was raised to 6, twice as high as that of the RADA16 peptide (pH 3–4), by replacing the strongly acidic aspartic acid with weakly acidic Glu and basic Thr in the RADA16 backbone. The results showed that RATEA16 had a stable β -sheet secondary structure, which could easily self-assemble into uniform nanofibers (70.3 nm in diameter and 273 nm in length) and eventually formed networks to trap the red blood cells, which

indicated the excellent self-assembling characteristic of RATEA16. RATEA16 possessed good biocompatibility, shorter blood coagulation initiation time and higher blood coagulation rate *in vitro*. RATEA16 was effective in reducing the time to hemostasis compared to CMS and Arista® in the rabbit liver wound model. The potent hemostatic effect of the prepared RATEA16 is attributed to the self-assembling characteristic of RATEA16, which favors trapping and sticking to red blood cells to rapidly form blood clots to stop the bleeding. The results proved that the RATEA16 peptide is a promising and ideal hemostatic agent with appropriate pH, shorter hemostasis time and good biocompatibility.

Conflicts of interest

There are no conflicts to declare.

Acknowledgements

This investigation was supported by the National Key Research and Development Program of China (No. 2016YFC1102900), the National Natural Science Foundation of China (No. 51772100), the Shanghai Pujiang Program (16PJD015) and the Joint Fund for equipment pre-research of the ministry of education (6141A02022618).

Notes and references

- 1 A. M. Behrens, M. J. Sikorski and P. Kofinas, *J. Biomed. Mater. Res., Part A*, 2014, **102**, 4182–4194.

- 2 G. de Gaetano, *Haematologica*, 2001, **86**, 349–356.
- 3 E. W. Davie, K. Fujikawa and W. Kisiel, *Biochemistry*, 1991, **30**, 10363–10370.
- 4 Z. Mirzakhani, K. Faghihi, A. Barati and H. R. Momeni, *J. Biomater. Sci., Polym. Ed.*, 2015, **26**, 1439–1451.
- 5 H. B. Alam, Z. Chen, A. Jaskille, R. I. Querol, E. Koustova, R. Inocencio, R. Conran, A. Seufert, N. Ariaban, K. Toruno and P. Rhee, *J. Trauma*, 2004, **56**, 974–983.
- 6 M. C. Neuffer, J. McDivitt, D. Rose, K. King, C. C. Cloonan and J. S. Vayer, *Mil. Med.*, 2004, **169**, 716–720.
- 7 W. D. Spotnitz, *World J. Surg.*, 2010, **34**, 632–634.
- 8 S. Subramaniam, K. Jurk, L. Hobohm, S. Jackel, M. Saffarzadeh, K. Schwierczek, P. Wenzel, F. Langer, C. Reinhardt and W. Ruf, *Blood*, 2017, **129**, 2291–2302.
- 9 M. B. Dowling, R. Kumar, M. A. Keibler, J. R. Hess, G. V. Bochicchio and S. R. Raghavan, *Biomaterials*, 2011, **32**, 3351–3357.
- 10 S. Y. Ong, J. Wu, S. M. Moochhala, M. H. Tan and J. Lu, *Biomaterials*, 2008, **29**, 4323–4332.
- 11 J. H. Ryu, Y. Lee, W. H. Kong, T. G. Kim, T. G. Park and H. Lee, *Biomacromolecules*, 2011, **12**, 2653–2659.
- 12 V. Shanmugam and M. H. Robinson, *Colorectal Dis.*, 2009, **11**, 221–222.
- 13 J. W. Carraway, D. Kent, K. Young, A. Cole, R. Friedman and K. R. Ward, *Resuscitation*, 2008, **78**, 230–235.
- 14 F. o. Arnaud, T. Tomori, W. Carr, A. McKeague, K. Teranishi, K. Prusaczyk and R. McCarron, *Ann. Biomed. Eng.*, 2008, **36**, 1708–1713.
- 15 W. D. Spotnitz, *Am. Surg.*, 2012, **78**, 1305–1321.
- 16 W. D. Spotnitz and S. Burks, *Transfusion*, 2008, **48**, 1502–1516.
- 17 J. R. Landry and I. O. Kanat, *J. Am. Podiatric Med. Assoc.*, 1985, **75**, 581–585.
- 18 R. G. Ellis-Behnke, Y. X. Liang, D. K. Tay, P. W. Kau, G. E. Schneider, S. Zhang, W. Wu and K. F. So, *Nanomedicine*, 2006, **2**, 207–215.
- 19 B. B. Hsu, W. Conway, C. M. Tschabrunn, M. Mehta, M. B. Perez-Cuevas, S. Zhang and P. T. Hammond, *ACS Nano*, 2015, **9**, 9394–9406.
- 20 L. Y.-H. Sang, Y.-X. Liang, Y. Li, W.-M. Wong, D. K.-C. Tay, K.-F. So, R. G. Ellis-Behnke, W. Wu and R. T.-F. Cheung, *Nanomedicine*, 2015, **11**, 611–620.
- 21 T. Wang, X. Zhong, S. Wang, F. Lv and X. Zhao, *Int. J. Mol. Sci.*, 2012, **13**, 15279–15290.
- 22 A. R. Cormier, C. Ruiz-Orta, R. G. Alamo and A. K. Paravastu, *Biomacromolecules*, 2012, **13**, 1794–1804.
- 23 Z. Ye, H. Zhang, H. Luo, S. Wang, Q. Zhou, X. Du, C. Tang, L. Chen, J. Liu, Y. K. Shi, E. Y. Zhang, R. Ellis-Behnke and X. Zhao, *J. Pept. Sci.*, 2008, **14**, 152–162.
- 24 H. Yokoi, T. Kinoshita and S. Zhang, *Proc. Natl. Acad. Sci. U. S. A.*, 2005, **102**, 8414–8419.
- 25 X. L. Wu, L. M. He, W. Li, H. Li, W. M. Wong, S. Ramakrishna and W. T. Wu, *Regener. Biomater.*, 2017, **4**, 21–30.
- 26 J. Guo, H. Su, Y. Zeng, Y. X. Liang, W. M. Wong, R. G. Ellis-Behnke, K. F. So and W. Wu, *Nanomedicine*, 2007, **3**, 311–321.
- 27 X. Liu, X. Wang, X. Wang, H. Ren, J. He, L. Qiao and F. Z. Cui, *Acta Biomater.*, 2013, **9**, 6798–6805.
- 28 Y. Sun, W. Li, X. Wu, N. Zhang, Y. Zhang, S. Ouyang, X. Song, X. Fang, R. Seeram, W. Xue, L. He and W. Wu, *ACS Appl. Mater. Interfaces*, 2016, **8**, 2348–2359.
- 29 S. Bag, S. Chaudhury, D. Pramanik, S. Dasgupta and S. Dasgupta, *Proteins: Struct., Funct., Bioinf.*, 2016, **84**, 1213–1223.
- 30 Y. Zhao, H. Yokoi, M. Tanaka, T. Kinoshita and T. Tan, *Biomacromolecules*, 2008, **9**, 1511–1518.
- 31 C. Dai, Y. Yuan, C. Liu, J. Wei, H. Hong, X. Li and X. Pan, *Biomaterials*, 2009, **30**, 5364–5375.
- 32 W. Zhang, D. Zhong, Q. Liu, Y. Zhang, N. Li, Q. Wang, Z. Liu and W. Xue, *J. Biomater. Sci., Polym. Ed.*, 2013, **24**, 1549–1563.
- 33 R. Wang, J. Li, W. Chen, T. Xu, S. Yun, Z. Xu, Z. Xu, T. Sato, B. Chi and H. Xu, *Adv. Funct. Mater.*, 2017, **27**, 1604894.
- 34 N. J. Greenfield, *Nat. Protoc.*, 2006, **1**, 2876–2890.
- 35 Y. Y. Choi, J. H. Jang, M. H. Park, B. G. Choi, B. Chi and B. Jeong, *J. Mater. Chem.*, 2010, **20**, 3416–3421.
- 36 S. Mangialardo, L. Gontrani, F. Leonelli, R. Caminiti and P. Postorino, *RSC Adv.*, 2012, **2**, 12329–12336.
- 37 J. H. Hong, H. J. Lee and B. Jeong, *ACS Appl. Mater. Interfaces*, 2017, **9**, 11568–11576.
- 38 L. Chronopoulou, S. Sennato, F. Bordi, D. Giannella, A. D. Nitto, A. Barbetta and C. Palocci, *Soft Matter*, 2014, **10**, 1944–1952.